

Semileptonic decays of Λ_c^+ in dynamical approaches

C. Q. Geng,^{1,2,3,4} Chong-Chung Lih,⁵ Chia-Wei Liu,³ and Tien-Hsueh Tsai³

¹*School of Fundamental Physics and Mathematical Sciences, Hangzhou Institute for Advanced Study, UCAS, Hangzhou 310024, China*

²*International Centre for Theoretical Physics Asia-Pacific, Beijing/Hangzhou, China*

³*Department of Physics, National Tsing Hua University, Hsinchu 300, Taiwan*

⁴*Physics Division, National Center for Theoretical Sciences, Hsinchu 300, Taiwan*

⁵*Department of Optometry, Central Taiwan University of Science and Technology, Taichung 406, Taiwan*



(Received 16 March 2020; accepted 4 May 2020; published 14 May 2020)

We study the semileptonic decays of $\Lambda_c^+ \rightarrow \Lambda(n)\ell^+\nu_\ell$ in two relativistic dynamical approaches of the light-front constituent quark model (LFCQM) and MIT bag model (MBM). By considering the Fermi statistic between quarks and determining spin-flavor structures in baryons along with the helicity formalism in the two different dynamical models, we calculate the branching ratios (\mathcal{B} s) and averaged asymmetry parameters (α s) in the decays. Explicitly, we find that $\mathcal{B}(\Lambda_c^+ \rightarrow \Lambda e^+\nu_e) = (3.36 \pm 0.87, 3.48)\%$ and $\alpha(\Lambda_c^+ \rightarrow \Lambda e^+\nu_e) = (-0.97 \pm 0.03, -0.83)$ in (LFCQM, MBM), in comparison with the data of $\mathcal{B}(\Lambda_c^+ \rightarrow \Lambda e^+\nu_e) = (3.6 \pm 0.4)\%$ and $\alpha(\Lambda_c^+ \rightarrow \Lambda e^+\nu_e) = -0.86 \pm 0.04$ given by the Particle Data Group, respectively. We also predict that $\mathcal{B}(\Lambda_c^+ \rightarrow n e^+\nu_e) = (0.57 \pm 0.15, 3.6 \pm 1.5) \times 10^{-3}$ and $\alpha(\Lambda_c^+ \rightarrow n e^+\nu_e) = (-0.98 \pm 0.02, -0.96 \pm 0.04)$ in LFCQM with two different scenarios for the momentum distributions of quarks in the neutron and $\mathcal{B}(\Lambda_c^+ \rightarrow n e^+\nu_e) = 0.279 \times 10^{-2}$ and $\alpha(\Lambda_c^+ \rightarrow n e^+\nu_e) = -0.87$ in MBM, which could be tested by the ongoing experiments at BESIII, LHCb, and BELLEII.

DOI: 10.1103/PhysRevD.101.094017

I. INTRODUCTION

Recently, the LHCb Collaboration has published the newest precision measurements on the antitriplet charmed baryon lifetimes [1], given by

$$\begin{aligned}\tau_{\Lambda_c^+} &= 203.5 \pm 1.0 \pm 1.3 \pm 1.4 \text{ fs}, \\ \tau_{\Xi_c^+} &= 456.8 \pm 3.5 \pm 2.9 \pm 3.1 \text{ fs}, \\ \tau_{\Xi_c^0} &= 154.5 \pm 1.7 \pm 1.6 \pm 1.0 \text{ fs}.\end{aligned}\quad (1)$$

Surprisingly, the lifetime of Ξ_c^0 given by LHCb magnificently deviates from the previous value of $\tau_{\Xi_c^0} = 112_{-10}^{+13}$ fs in the work by the Particle Data Group (PDG) [2]. Meanwhile, the Belle Collaboration has measured the absolute branching ratios of $\mathcal{B}(\Xi_c^0 \rightarrow \Xi^- \pi^+) = (1.8 \pm 0.5)\%$ [3] and $\mathcal{B}(\Xi_c^+ \rightarrow \Xi^- \pi^+ \pi^+) = (2.86 \pm 1.21 \pm 0.38)\%$ [4], which are the golden modes to determine other $\Xi_c^{0,+}$ decay channels, respectively. It is clear that we are now witnessing a new era of charm physics. One can expect that there will be

more and more new experimental data and precision measurements in the near future, which are also the guiding light for people to explore new physics beyond the standard model.

There have recently been many works discussing the antitriplet charm baryon decays. Because of the complicated baryon structures, particularly the large nonperturbative effects in the QCD, it is very hard to calculate the baryonic decay amplitudes from first principles. In the literature, people use the flavor symmetry of $SU(3)_f$ to analyze various charmed baryon decay processes, such as semileptonic and two-body and three-body nonleptonic decays, to obtain reliable results [5–25]. However, the $SU(3)_f$ symmetry is an approximate symmetry, resulting in about 10% of errors for the predictions naturally. To have more precise calculations, we need a dynamical QCD model to understand each process. For simplicity, we only discuss the semileptonic processes, which involve purely the factorizable effects without the nonfactorizable ones. In particular, we focus on the Λ_c^+ semileptonic decays in this work. There are several theoretical analyses and lattice QCD (LQCD) calculations on the charmed baryon semileptonic decays with different dynamical models in the literature [26–33]. In this paper, we will mainly use the light-front (LF) formalism to study the decays and check the results in the MIT bag model (MBM) as comparisons.

Published by the American Physical Society under the terms of the [Creative Commons Attribution 4.0 International license](https://creativecommons.org/licenses/by/4.0/). Further distribution of this work must maintain attribution to the author(s) and the published article's title, journal citation, and DOI. Funded by SCOAP³.

The LF formalism is considered as a consistent relativistic approach, which has been very successful in the mesonic sectors [34,35]. Because of this success, it has been extended to other systems, such as those involving the heavy mesons, pentaquarks, and so on [36–47]. In addition, the bottom baryon to charmed baryon nonleptonic decays in the LF approach have been done in Refs. [48,49]. For a review on the nonperturbative nature in the equation of motion and QCD vacuum structure for the LF constituent quark model (LFCQM), one can refer to the article of Ref. [34]. The advantage of LFCQM is that the commutativity of the LF Hamiltonian and boost generators provide us with good convenience to calculate the wave function in different inertial frames because of the recoil effect.

The MBM is a QCD-inspired phenomenological model. In the MBM, a baryon is described as three free quarks with current masses confined in a spherical bag with a bag size R . This simple and intuitive picture helps people to deal with the interactions between hadrons as well as their mass spectra. The authors in Ref. [33] calculated all $c \rightarrow s/d$ baryonic transition form factors at zero-recoiled points and

discussed both the monopole and dipole behaviors, and others in Refs. [50–52] have further combined the MBM with the pole model and current algebra to predict various charmed baryon nonleptonic decays.

This paper is organized as follows. We present our formal calculations of the baryonic transition form factors for LFCQM and MBM in Secs. II and III, respectively. We show our numerical results of the form factors, branching ratios, and averaged asymmetry parameters in Sec. IV. We also compare our results with those in the literature. In Sec. V, we give our conclusions.

II. BARYONIC TRANSITION FORM FACTORS IN LFCQM

A. Vertex function of baryon

In LFCQM, a baryon with its momentum P and spin S as well as the z-direction projection of spin S_z are considered as a bound state of three constitute quarks. As a result, the baryon state can be expressed by [34,35,42,53–55]

$$|\mathbf{B}, P, S, S_z\rangle = \int \{d^3\tilde{p}_1\}\{d^3\tilde{p}_2\}\{d^3\tilde{p}_3\} 2(2\pi)^3 \frac{1}{\sqrt{P^+}} \delta^3(\tilde{P} - \tilde{p}_1 - \tilde{p}_2 - \tilde{p}_3) \times \sum_{\lambda_1, \lambda_2, \lambda_3} \Psi^{SS_z}(\tilde{p}_1, \tilde{p}_2, \tilde{p}_3, \lambda_1, \lambda_2, \lambda_3) C^{a\beta\gamma} F_{abc} |q_a^a(\tilde{p}_1, \lambda_1) q_\beta^b(\tilde{p}_2, \lambda_2) q_\alpha^c(\tilde{p}_3, \lambda_3)\rangle, \quad (2)$$

where $\Psi^{SS_z}(\tilde{p}_1, \tilde{p}_2, \tilde{p}_3, \lambda_1, \lambda_2, \lambda_3)$ is the vertex function, which can be formally solved from the Bethe-Salpeter equations by the Faddeev decomposition method; $C^{a\beta\gamma}$ and F_{abc} are the color and flavor factors; and λ_i and \tilde{p}_i with $i = 1, 2, 3$ are the LF helicities and 3-momenta of the on-mass-shell constituent quarks, defined as

$$\tilde{p}_i = (p_i^+, p_{i\perp}), \quad p_{i\perp} = (p_i^1, p_i^2), \quad p_i^- = \frac{m_i^2 + p_{i\perp}^2}{p_i^+}, \quad (3)$$

and

$$d^3\tilde{p}_i \equiv \frac{dp_i^+ d^2p_{i\perp}}{2(2\pi)^3}, \quad \delta^3(\tilde{p}) = \delta(p^+) \delta^2(p_\perp), \quad |q_\alpha^a(\tilde{p}, \lambda)\rangle = d_\alpha^{*a}(\tilde{p}, \lambda)|0\rangle, \quad \{d_\alpha^{a'}(\tilde{p}', \lambda'), d_\alpha^{*a}(\tilde{p}, \lambda)\} = 2(2\pi)^3 \delta^3(\tilde{p}' - \tilde{p}) \delta_{\lambda'\lambda} \delta_{\alpha'a} \delta^{a'a}, \quad (4)$$

respectively. To describe the internal motions of the constituent quarks, we introduce the kinematic variables of (q_\perp, ξ) , (Q_\perp, η) , and P_{tot} , given by

$$P_{\text{tot}} = \tilde{P}_1 + \tilde{P}_2 + \tilde{P}_3, \quad \xi = \frac{p_1^+}{p_1^+ + p_2^+}, \quad \eta = \frac{p_1^+ + p_2^+}{P_{\text{tot}}^+}, \quad q_\perp = (1 - \xi)p_{1\perp} - \xi p_{2\perp}, \quad Q_\perp = (1 - \eta)(p_{1\perp} + p_{2\perp}) - \eta p_{3\perp}, \quad (5)$$

where (q_\perp, ξ) characterize the relative motion between the first and second quarks, while (Q_\perp, η) characterize the third and other two quarks. The invariant masses of (q_\perp, ξ) and (Q_\perp, η) systems are represented by [35]

$$M_3^2 = \frac{q_\perp^2}{\xi(1 - \xi)} + \frac{m_1^2}{\xi} + \frac{m_2^2}{1 - \xi}, \quad M^2 = \frac{Q_\perp^2}{\eta(1 - \eta)} + \frac{M_3^2}{\eta} + \frac{m_3^2}{1 - \eta}, \quad (6)$$

respectively. Unlike Refs. [53–55], which treat the diquark as a pointlike object or spectator, we consider the three constituent quarks in the baryon independently with suitable quantum numbers satisfying the Fermi statistics to have a correct baryon bound state system. The vertex function of $\Psi^{SS_z}(\tilde{p}_1, \tilde{p}_2, \tilde{p}_3, \lambda_1, \lambda_2, \lambda_3)$ in Eq. (2) can be written as [34,35,56]

$$\Psi^{SS_z}(\tilde{p}_1, \tilde{p}_2, \tilde{p}_3, \lambda_1, \lambda_2, \lambda_3) = \Phi(q_\perp, \xi, Q_\perp, \eta) \Xi^{SS_z}(\lambda_1, \lambda_2, \lambda_3), \quad (7)$$

where $\Phi(q_\perp, \xi, Q_\perp, \eta)$ is the momentum distribution of constituent quarks and $\Xi^{SS_z}(\lambda_1, \lambda_2, \lambda_3)$ represents the momentum-dependent spin wave function, given by

$$\Xi^{SS_z}(\lambda_1, \lambda_2, \lambda_3) = \sum_{s_1, s_2, s_3} \langle \lambda_1 | R_1^\dagger | s_1 \rangle \langle \lambda_2 | R_2^\dagger | s_2 \rangle \langle \lambda_3 | R_3^\dagger | s_3 \rangle \left\langle \frac{1}{2} s_1, \frac{1}{2} s_2, \frac{1}{2} s_3 \left| SS_z \right. \right\rangle, \quad (8)$$

with $\langle \frac{1}{2} s_1, \frac{1}{2} s_2, \frac{1}{2} s_3 | SS_z \rangle$ the usual $SU(2)$ Clebsch-Gordan coefficient and R_i the well-known Melosh transformation, which corresponds to the i th constituent quark, expressed by

$$\begin{aligned} R_1 &= R_M(\eta, Q_\perp, M_3, M) R_M(\xi, q_\perp, m_1, M_3), \\ R_2 &= R_M(\eta, Q_\perp, M_3, M) R_M(1 - \xi, -q_\perp, m_2, M_3), \\ R_3 &= R_M(1 - \eta, -Q_\perp, m_3, M), \end{aligned} \quad (9)$$

with

$$R_M(x, p_\perp, m, M) = \frac{m + xM - i\vec{\sigma} \cdot (\vec{n} \times \vec{q})}{\sqrt{(m + xM)^2 + q_\perp^2}}, \quad (10)$$

where $\vec{\sigma}$ stands for the Pauli matrix and $\vec{n} = (0, 0, 1)$. This is the generalization of the Melosh transformation from two-particle systems, which can be derived from the transformation property of angular momentum operators [35,57]. We further represent the LF kinematic variables (ξ, q_\perp) and (η, Q_\perp) in the forms of the ordinary 3-momenta \mathbf{q} and \mathbf{Q} ,

$$\begin{aligned} E_{1(2)} &= \sqrt{\mathbf{q}^2 + m_{1(2)}^2}, & E_{12} &= \sqrt{\mathbf{Q}^2 + M_3^2}, \\ E_3 &= \sqrt{\mathbf{Q}^2 + m_3^2}, & q_z &= \frac{\xi M_3}{2} - \frac{m_1^2 + q_\perp^2}{2M_3\xi}, \\ Q_z &= \frac{\eta M}{2} - \frac{M_3^2 + Q_\perp^2}{2M\eta}, \end{aligned} \quad (11)$$

to get more clear physical pictures of the momentum distribution wave functions.

It is known that the exact momentum wave function cannot be solved from the first principle currently due to the lack of knowledge about the effective potential in the three-body system in QCD. Hence, we choose the phenomenological Gaussian-type wave function with suitable shape parameters to include the diquark clustering effects in Λ_c^+ and Λ baryons [35,53]. The baryon spin-flavor-momentum wave function $F_{abc} \Psi^{SS_z}(\tilde{p}_1, \tilde{p}_2, \tilde{p}_3, \lambda_1, \lambda_2, \lambda_3)$ should be totally symmetric under any permutations of quarks to keep the Fermi statistics. The spin-flavor-momentum wave functions of Λ_c^+ , Λ , and n are given by

$$\begin{aligned} |\Lambda_c\rangle &= \frac{1}{\sqrt{6}} [\phi_3 \chi^{\rho^3} (|duc\rangle - |udc\rangle) + \phi_2 \chi^{\rho^2} (|dcu\rangle - |ucd\rangle) \\ &\quad + \phi_1 \chi^{\rho^1} (|cdu\rangle - |cud\rangle)], \\ |\Lambda\rangle &= \frac{1}{\sqrt{6}} [\phi_3 \chi^{\rho^3} (|duc\rangle - |uds\rangle) + \phi_2 \chi^{\rho^2} (|dsu\rangle - |usd\rangle) \\ &\quad + \phi_1 \chi^{\rho^1} (|sdu\rangle - |sud\rangle)], \\ |n\rangle &= \frac{1}{\sqrt{3}} \phi [\chi^{\lambda^3} |ddu\rangle + \chi^{\lambda^2} |dud\rangle + \chi^{\lambda^1} |udd\rangle], \end{aligned} \quad (12)$$

respectively, where

$$\begin{aligned} \chi_\uparrow^{\rho^3} &= \frac{1}{\sqrt{2}} (|\uparrow\downarrow\uparrow\rangle - |\downarrow\uparrow\uparrow\rangle), \\ \chi_\uparrow^{\lambda^3} &= \frac{1}{\sqrt{6}} (|\uparrow\downarrow\uparrow\rangle + |\downarrow\uparrow\uparrow\rangle - 2|\uparrow\uparrow\downarrow\rangle), \\ \phi_3 &= \mathcal{N} \sqrt{\frac{\partial q_z}{\partial \xi} \frac{\partial Q_z}{\partial \eta} e^{-\frac{\mathbf{Q}^2}{2\beta_Q^2} - \frac{q_\perp^2}{2\beta_q^2}}}, \end{aligned} \quad (13)$$

and $\phi_{1(2)}$ has the form by replacing (\mathbf{q}, \mathbf{Q}) with $(\mathbf{q}_{1(2)}, \mathbf{Q}_{1(2)})$ in ϕ_3 , with $\mathcal{N} = 2(2\pi)^3 (\beta_q \beta_Q \pi)^{-3/2}$ and $\beta_{q,Q}$ being the normalized constant and shape parameters, respectively. Explicitly, $\mathbf{q}_{1(2)}$ and $\mathbf{Q}_{1(2)}$ are given by

$$\begin{aligned} \xi_{1(2)} &= \frac{p_{2(3)}^+}{p_{2(3)}^+ + p_1^+}, & \eta_{1(2)} &= 1 - \frac{p_{1(2)}^+}{P_{\text{tot}}^+}, \\ q_{1(2)\perp} &= (1 - \xi_{1(2)}) p_{2(3)\perp} - \xi_{1(2)} p_{3(1)\perp}, \\ Q_{1(2)\perp} &= (1 - \eta_{1(2)}) (p_{2(3)\perp} + p_{3(1)\perp}) - \eta_{1(2)} p_{1(2)\perp}. \end{aligned} \quad (14)$$

Here, the baryon state is normalized as

$$\langle \mathbf{B}, P', S', S'_z | \mathbf{B}, P, S, S_z \rangle = 2(2\pi)^3 P^+ \delta^3(\vec{P}' - \vec{P}) \delta_{S'_z S_z}, \quad (15)$$

resulting in the normalization of the momentum wave function, given by

$$\frac{1}{2^2(2\pi)^6} \int d\xi_{(1,2)} d\eta_{(1,2)} d^2 q_{(1,2)\perp} d^2 Q_{(1,2)\perp} |\phi_{3(1,2)}|^2 = 1. \quad (16)$$

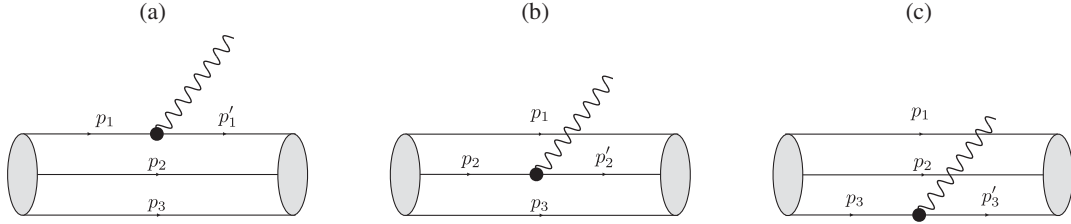


FIG. 1. Feynman diagrams for the baryonic weak transitions at the lowest order, where the sign of “Bullet symbol” denotes the V-A current vertex, with (a) $p'_1 - p_1 = k$, (b) $p'_2 - p_2 = k$, and (c) $p'_3 - p_3 = k$.

We emphasize that the momentum wave functions of ϕ_i with the different shape parameters of β_q and β_Q describe the scalar diquark effects in $\Lambda_{(c)}$. For the neutron, the momentum distribution functions are the same, i.e., $\phi = \phi_3(\beta_q = \beta_Q)$, for any spin-flavor state due to the isospin symmetry. Note that there is no $SU(6)$ spin-flavor symmetry in $\Lambda_{(c)}$ even though the forms of these states are similar to those with $SU(6)$.

B. Transition form factors

The baryonic transition form factors of the $V - A$ weak current are defined by

$$\begin{aligned} & \langle \mathbf{B}_f, P', S', S'_z | \bar{q} \gamma^\mu (1 - \gamma_5) c | \mathbf{B}_i, P, S, S_z \rangle \\ &= \bar{u}_{\mathbf{B}_f}(P', S'_z) \left[\gamma^\mu f_1(k^2) - i \sigma^{\mu\nu} \frac{k_\nu}{M_{\mathbf{B}_i}} f_2(k^2) \right. \\ & \quad \left. + \frac{k^\mu}{M_{\mathbf{B}_i}} f_3(k^2) \right] u_{\mathbf{B}_i}(P, S_z) - \bar{u}_{\mathbf{B}_f}(P', S'_z) \left[\gamma^\mu g_1(k^2) \right. \\ & \quad \left. - i \sigma^{\mu\nu} \frac{k_\nu}{M_{\mathbf{B}_i}} g_2(k^2) + \frac{k^\mu}{M_{\mathbf{B}_i}} g_3(k^2) \right] \gamma_5 u_{\mathbf{B}_i}(P, S_z), \quad (17) \end{aligned}$$

where $\sigma^{\mu\nu} = \frac{i}{2} [\gamma^\mu, \gamma^\nu]$ and $P' - P = k$. We choose the frame such that P^+ is conserved ($k^+ = 0, k^2 = -k_\perp^2$) to calculate the form factors to avoid other x^+ -ordered diagrams in the LF formalism [35]. The matrix elements of the vector and

axial-vector currents at quark level correspond to three different lowest-order Feynman diagrams as shown in Fig. 1. Since the spin-flavor-momentum wave functions of baryons are totally symmetric under the permutation of quarks, we have that $(a) + (b) + (c) = 3(a) = 3(b) = 3(c)$ [35]. For an illustration, we only present the calculation for the diagram (c), which contains simpler and cleaner forms with the notation $(q_\perp, Q_\perp, \xi, \eta)$. We can extract the form factors from the matrix elements through the relations

$$\begin{aligned} f_1(k^2) &= \frac{1}{2P^+} \langle \mathbf{B}_f, P', \uparrow | \bar{q} \gamma^+ c | \mathbf{B}_i, P, \uparrow \rangle, \\ f_2(k^2) &= \frac{1}{2P^+} \frac{M_{\mathbf{B}_i}}{k_\perp} \langle \mathbf{B}_f, P', \uparrow | \bar{q} \gamma^+ c | \mathbf{B}_i, P, \downarrow \rangle, \\ g_1(k^2) &= \frac{1}{2P^+} \langle \mathbf{B}_f, P', \uparrow | \bar{q} \gamma^+ \gamma_5 c | \mathbf{B}_i, P, \uparrow \rangle, \\ g_2(k^2) &= \frac{1}{2P^+} \frac{M_{\mathbf{B}_i}}{k_\perp} \langle \mathbf{B}_f, P', \uparrow | \bar{q} \gamma^+ \gamma_5 c | \mathbf{B}_i, P, \downarrow \rangle. \quad (18) \end{aligned}$$

Note that f_3 and g_3 cannot be obtained when $k^+ = 0$, but they are negligible because of the suppressions of the k^2 factors. In addition, the terms associated with f_3 and g_3 do not contribute to the semileptonic decays [22]. As a result, we set both f_3 and g_3 to be 0 in this study. With the help of the momentum distribution functions and the Melosh transformation matrix, the transition matrix elements can be expressed as

$$\begin{aligned} \langle \mathbf{B}_f, P', S', S'_z | \bar{q} \gamma^+ c | \mathbf{B}_i, P, S, S_z \rangle &= \frac{1}{2^2 (2\pi)^6} \int d\xi d\eta d^2 q_\perp d^2 Q_\perp \Phi(q'_\perp, \xi, Q'_\perp, \eta) \Phi(q_\perp, \xi, Q_\perp, \eta) F^{def} F_{abc} \delta_d^a \delta_e^b \\ & \times \sum_{s_1, s_2, s_3} \sum_{s'_1, s'_2, s'_3} \langle S', S'_z | s'_1, s'_2, s'_3 \rangle \langle s_1, s_2, s_3 | S, S_z \rangle \langle s'_1 | R'_1 R'_1^\dagger | s_1 \rangle \langle s'_2 | R'_2 R'_2^\dagger | s_2 \rangle \\ & \times 2P^+ \sum_{\lambda'_3, \lambda_3} \langle s'_3 | R'_3 | \lambda'_3 \rangle (\delta_{q_f q} 3 \delta_{\lambda'_3 \lambda_3} \delta_{c q^c}) \langle \lambda_3 | R_3^\dagger | s_3 \rangle, \quad (19) \end{aligned}$$

$$\begin{aligned} \langle \mathbf{B}_f, P', S', S'_z | \bar{q} \gamma^+ \gamma_5 c | \mathbf{B}_i, P, S, S_z \rangle &= \frac{1}{2^2 (2\pi)^6} \int d\xi d\eta d^2 q_\perp d^2 Q_\perp \Phi(q'_\perp, \xi, Q'_\perp, \eta) \Phi(q_\perp, \xi, Q_\perp, \eta) F^{def} F_{abc} \delta_d^a \delta_e^b \\ & \times \sum_{s_1, s_2, s_3} \sum_{s'_1, s'_2, s'_3} \langle S', S'_z | s'_1, s'_2, s'_3 \rangle \langle s_1, s_2, s_3 | S, S_z \rangle \langle s'_1 | R'_1 R'_1^\dagger | s_1 \rangle \langle s'_2 | R'_2 R'_2^\dagger | s_2 \rangle \\ & \times 2P^+ \sum_{\lambda'_3, \lambda_3} \langle s'_3 | R'_3 | \lambda'_3 \rangle (\delta_{q_f q} 3 (\sigma_z)_{\lambda'_3 \lambda_3} \delta_{c q^c}) \langle \lambda_3 | R_3^\dagger | s_3 \rangle. \quad (20) \end{aligned}$$

Using Eqs. (18), (19), and (20), we find that

$$f_1(k^2) = \frac{3}{2^2(2\pi)^6} \int d\xi d\eta d^2q_\perp d^2Q_\perp \Phi(q'_\perp, \xi, Q'_\perp, \eta) \Phi(q_\perp, \xi, Q_\perp, \eta) (F^{def} F_{abc} \delta_{q_f q} \delta_{c q^c} \delta_d^a \delta_e^b) \\ \times \sum_{s_1, s_2, s_3} \sum_{s'_1, s'_2, s'_3} \langle S', \uparrow | s'_1, s'_2, s'_3 \rangle \langle s_1, s_2, s_3 | S, \uparrow \rangle \prod_{i=1,2,3} \langle s'_i | R'_i R_i^\dagger | s_i \rangle, \quad (21)$$

$$g_1(k^2) = \frac{3}{2^2(2\pi)^6} \int d\xi d\eta d^2q_\perp d^2Q_\perp \Phi(q'_\perp, \xi, Q'_\perp, \eta) \Phi(q_\perp, \xi, Q_\perp, \eta) (F^{def} F_{abc} \delta_{q_f q} \delta_{c q^c} \delta_d^a \delta_e^b) \\ \times \sum_{s_1, s_2, s_3} \sum_{s'_1, s'_2, s'_3} \langle S', \uparrow | s'_1, s'_2, s'_3 \rangle \langle s_1, s_2, s_3 | S, \uparrow \rangle \prod_{i=1,2} \langle s'_i | R'_i R_i^\dagger | s_i \rangle \langle s'_3 | R'_3 \sigma_z R_3^\dagger | s_3 \rangle, \quad (22)$$

$$f_2(k^2) = \frac{3}{2^2(2\pi)^6} \frac{M_{B_i}}{k_\perp} \int d\xi d\eta d^2q_\perp d^2Q_\perp \Phi(q'_\perp, \xi, Q'_\perp, \eta) \Phi(q_\perp, \xi, Q_\perp, \eta) (F^{def} F_{abc} \delta_{q_f q} \delta_{c q^c} \delta_d^a \delta_e^b) \\ \times \sum_{s_1, s_2, s_3} \sum_{s'_1, s'_2, s'_3} \langle S', \uparrow | s'_1, s'_2, s'_3 \rangle \langle s_1, s_2, s_3 | S, \downarrow \rangle \prod_{i=1,2,3} \langle s'_i | R'_i R_i^\dagger | s_i \rangle, \quad (23)$$

$$g_2(k^2) = \frac{3}{2^2(2\pi)^6} \frac{M_{B_i}}{k_\perp} \int d\xi d\eta d^2q_\perp d^2Q_\perp \Phi(q'_\perp, \xi, Q'_\perp, \eta) \Phi(q_\perp, \xi, Q_\perp, \eta) (F^{def} F_{abc} \delta_{q_f q} \delta_{c q^c} \delta_d^a \delta_e^b) \\ \times \sum_{s_1, s_2, s_3} \sum_{s'_1, s'_2, s'_3} \langle S', \uparrow | s'_1, s'_2, s'_3 \rangle \langle s_1, s_2, s_3 | S, \downarrow \rangle \prod_{i=1,2} \langle s'_i | R'_i R_i^\dagger | s_i \rangle \langle s'_3 | R'_3 \sigma_z R_3^\dagger | s_3 \rangle. \quad (24)$$

III. BARYONIC TRANSITION FORM FACTORS IN MBM

The formalism for MBM can be found in Ref. [33]. In the calculation of MBM, we take the same notations as those in Ref. [33]. In this approach, the current quark masses are used, given by

$$m_{u,d} = 0.005 \text{ GeV}, \quad m_s = 0.28 \text{ GeV}, \\ m_c = 1.5 \text{ GeV}, \quad R = 5 \text{ GeV}^{-1}, \quad (25)$$

where R corresponds to the bag size, which is valid at least for the charmed baryons [58–61]. Note that the form factors can only be evaluated at $\vec{k} = 0$ ($k^2 = (M_1 - M_2)^2$). For $\vec{k} \neq 0$, the bag is not at the rest frame of the initial baryon, and we will face the problem of how to boost the state in MBM, which is very subtle and beyond the study of this work [62]. The form factors are decomposed as

$$f_1 = \mathcal{V}_0 - \mathcal{V}_M \Delta M^2 / M_{12} - \mathcal{V}_V \Delta M, \\ f_2 = (-\mathcal{V}_0 + \mathcal{V}_M M_{12} + \mathcal{V}_V \Delta M) M_1 / M_{12}, \\ g_1 = (1 - \Delta M^2 / 2M_{12}^2) \mathcal{A}_s + (\mathcal{A}_T \Delta M - \mathcal{A}_0) 4M_1 M_2 \Delta M / M_{12}^2, \\ g_2 = (\mathcal{A}_T \Delta M - \mathcal{A}_s \Delta M / 8M_1 M_2 - \mathcal{A}_0) 4M_1^2 M_2 / M_{12}^2, \quad (26)$$

with $\Delta M = M_1 - M_2$, $M_{12} = M_1 + M_2$, and

$$\mathcal{V}_0 = AR^3 (W_+^i W_+^f I_{00} + W_-^i W_-^f I_{11}), \\ \mathcal{V} = AR^3 (W_-^i W_+^f I_{10} - W_+^i W_-^f I_{01}) (R/3), \\ \mathcal{V}_M = AR^3 (W_-^i W_+^f I_{10} + W_+^i W_-^f I_{01}) (R/3), \\ \mathcal{A}_0 = AR^3 (W_-^i W_+^f I_{10} - W_+^i W_-^f I_{01}) (R/3), \\ \mathcal{A}_s = AR^3 (W_+^i W_+^f - W_-^i W_-^f I_{11}/3), \\ \mathcal{A}_T = AR^3 W_-^i W_-^f J_{11} (-2R^2/15), \quad (27)$$

where A is the normalized factor for the baryon, corresponding to the baryon spin-flavor structures in Table II of Ref. [33]; W_\pm^q are associated with the normalized factors for quarks, given by

$$W_\pm^q \equiv \left(\frac{\omega^q \pm m_q}{\omega^q} \right)^{1/2} \quad (28)$$

with $q = i$ or f the quark flavor and ω^q the quark energy; and I and J stand for the overlap factors for the quark wave functions, defined by

$$I_{nn} \equiv \int_0^1 dt t^2 j_n(tx_0^i) j_n(tx_0^f), \quad n = 0, 1 \\ I_{nm} \equiv \int_0^1 dt t^3 j_n(tx_0^i) j_m(tx_0^f), \quad n, m = 0, 1 \quad (n \neq m) \\ J_{11} \equiv \int_0^1 dt t^4 j_1(tx_0^i) j_1(tx_0^f), \quad (29)$$

TABLE I. Values of the constituent quark masses (m_i) and shape parameters (β_{qB} and β_{QB}) in units of GeV, where $\beta_{I,II} = \beta_{Qn} = \beta_{qn}$.

m_c	m_s	m_d	m_c	$\beta_{q\Lambda_c}$	$\beta_{Q\Lambda_c}$	$\beta_{q\Lambda}$	$\beta_{Q\Lambda}$	$\beta_{I,II}$
1.3	0.4	0.26	0.26	0.44	0.54	0.44	0.37	0.22,0.44

with j_n the Bessel function and x_0^q the lowest root of the transcendental equation of

$$\tan(x^q) = \frac{x^q}{1 - m_q R - [(x^q)^2 + (m_q R)^2]^{1/2}}. \quad (30)$$

IV. NUMERICAL RESULTS

As shown in Sec. II, the baryonic transition form factors in LFCQM can be evaluated only in the spacelike region ($k^2 = -k_{\perp}^2$) because of the condition $k^+ = 0$. Thus, we follow the standard procedures in Refs. [41,42,54] to extract the information of the form factors in the timelike region. These procedures have widely been tested and discussed in the mesonic sector [63,64]. We fit $f_{1(2)}(k^2)$ and $g_{1(2)}(k^2)$ with some analytic functions in the spacelike region, which are analytically continued to the physical timelike region ($k^2 > 0$). We employ the numerical values of the constituent quark masses and shape parameters in Table I. The values of the shape parameters can be determined approximately by the calculations in the mesonic sectors [53,65]. Since the strength of the quark-quark (qq') potential is a half of the quark-antiquark $q\bar{q}'$ one, the shape parameters of the quark pairs β_{qB} should be $\sqrt{2}$ smaller than those in the mesonic sectors [53]. Meanwhile, the reciprocals of the shape parameters are related to the sizes of systems. Consequently, we adopt $\beta_{q\Lambda_{(c)}} \simeq 2(\beta_{u\bar{d}}/\sqrt{2})$, where the factor of 2 is used to parametrize the effects of the diquark clusterings, resulting in the light quark pairs to be more compact. For the quark-diquark shape parameters $\beta_{Q\Lambda_{(c)}}$, we choose the values of $\beta_{s(c)\bar{s}}$ without any additional factors. The diquark cluster effectively forms a color antitriplet and hence shares the same potential strength as the $q\bar{q}'$ one. Finally, because of the isospin symmetry, all constitute quarks in the neutron are expected to have the same momentum distribution, so that the shape parameters are $\beta_{Qn} = \beta_{qn} = \beta$. We use two scenarios for β to describe the quarks in the neutron. The first one is from the harmonic oscillator picture, which leads to $\beta_I = \beta_{u\bar{d}}/\sqrt{2} \simeq 0.22$ GeV through the quark-quark interaction, in which the value of 0.22 GeV is consistent with $R = 5$ GeV $^{-1}$ in the MIT bag model. The other one is to maintain the shape parameters of $\beta_{q\Lambda_{(c)}}$ to be the same, i.e., $\beta_{II} = \beta_{Qn} = \beta_{qn} = \beta_{q\Lambda_c} = 0.44$ GeV. By using Eqs. (21)–(24), we compute totally 32 points for all form factors from $k^2 = 0$ to $k^2 = -9.7$ GeV 2 . With the MATLAB

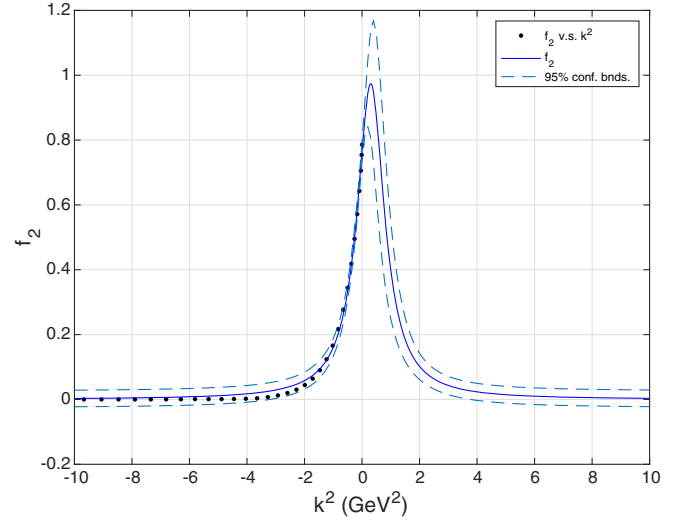
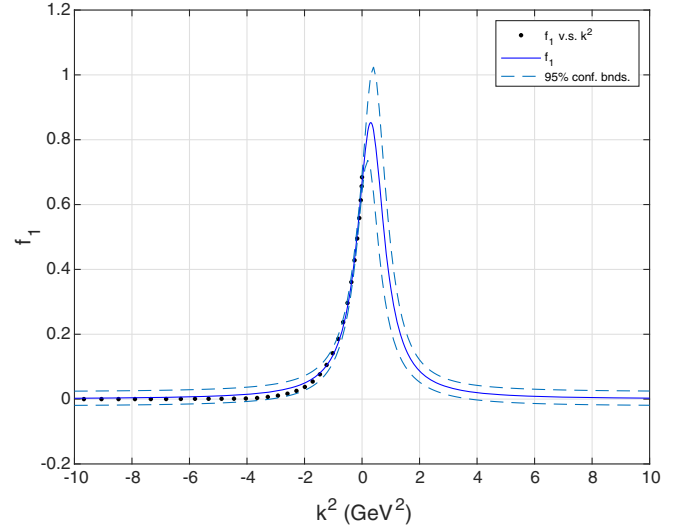


FIG. 2. Vector form factors of $f_{1,2}$ with respect to the transfer momentum k^2 in unit of GeV 2 for $\Lambda_c^+ \rightarrow \Lambda$.

curve fitting toolbox, we present our results of $\Lambda_c^+ \rightarrow \Lambda$ in Figs. 2 and 3 and $\Lambda_c^+ \rightarrow n$ in Figs. 4 and 5 based on 95% confidence bounds given in Appendix, respectively. To fit the k^2 dependences of the form factors in the spacelike region, we use the form

$$F(k^2) = \frac{F(0)}{1 - q_1 k^2 + q_2 k^4}. \quad (31)$$

We present our fitting results in Table II.

For the MBM, we assume the k^2 dependence of the form factors as

$$\begin{aligned} f_i(k^2) &= \frac{(1 + d_f)f_i(0)}{(1 - \frac{k^2}{M_V^2})^2 + d_f} \\ g_i(k^2) &= \frac{(1 + d_g)g_i(0)}{(1 - \frac{k^2}{M_A^2})^2 + d_g} \end{aligned} \quad (32)$$

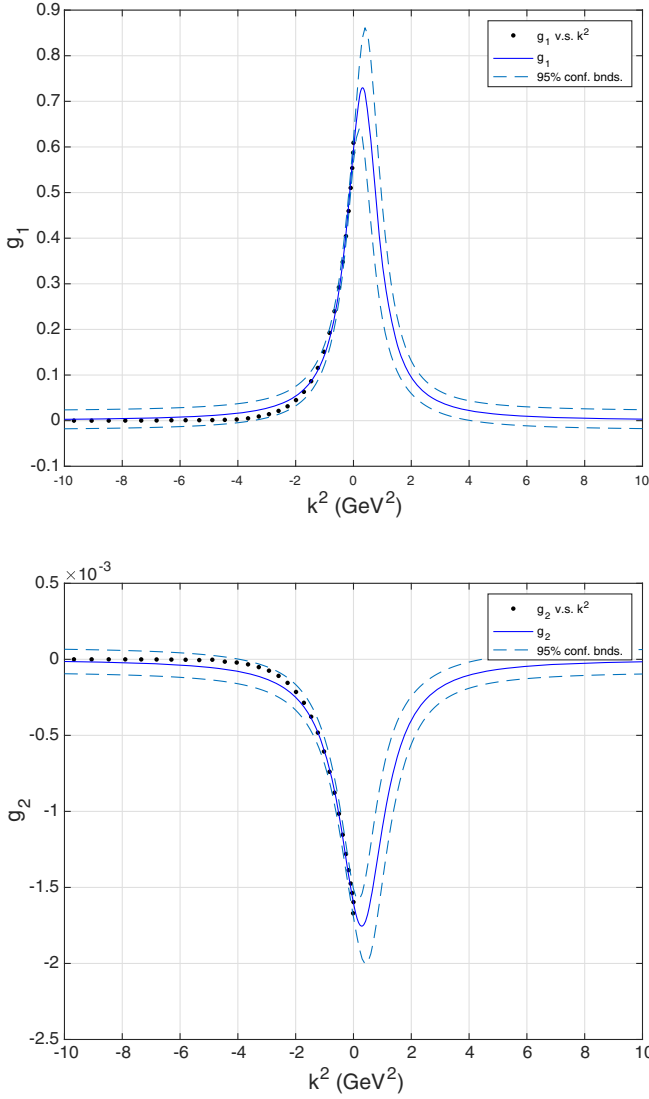


FIG. 3. Axial-vector form factors of $g_{1,2}$ with respect to the transfer momentum k^2 in unit of GeV^2 in $\Lambda_c^+ \rightarrow \Lambda$.

where $M_V=2.112(2.010)\text{GeV}$ and $M_A=2.556(2.423)\text{GeV}$, while d_f and d_g are fitted to be 0.2 and $d_g = 0.1$, respectively. We will call the k^2 -dependent forms in Eq. (32) the Lorentzian type. We list $f_i(0) = f_i$ and $g_i(0) = g_i$ in Table III.

To calculate the decay branching ratios and other physical quantities, we introduce the helicity amplitudes of $H_{\lambda_2 \lambda_w}^{V(A)}$, which give more intuitive physical pictures and simpler expressions when discussing the asymmetries of the decay processes, such as the integrated (averaged) asymmetry, also known as the longitudinal polarization of the daughter baryon. Relations between the helicity amplitudes and form factors are given by

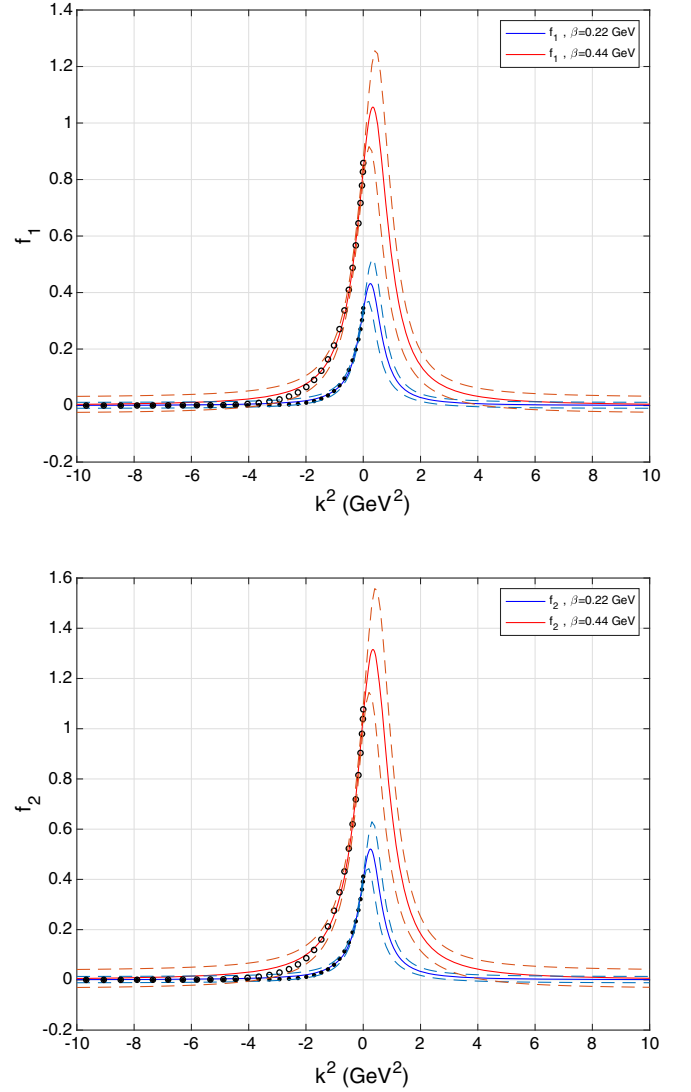


FIG. 4. Legend is the same as Fig. 2 but for $\Lambda_c^+ \rightarrow n$.

$$\begin{aligned}
 H_{\frac{1}{2}1}^V &= \sqrt{2K_-} \left(-f_1 - \frac{M_{\mathbf{B}_i} + M_{\mathbf{B}_f}}{M_{\mathbf{B}_i}} f_2 \right), \\
 H_{\frac{1}{2}0}^V &= \frac{\sqrt{K_-}}{\sqrt{k^2}} \left((M_{\mathbf{B}_i} + M_{\mathbf{B}_f}) f_1 + \frac{k^2}{M_{\mathbf{B}_i}} f_2 \right), \\
 H_{\frac{1}{2}f}^V &= \frac{\sqrt{K_+}}{\sqrt{k^2}} \left((M_{\mathbf{B}_i} + M_{\mathbf{B}_f}) f_1 + \frac{k^2}{M_{\mathbf{B}_i}} f_3 \right), \\
 H_{\frac{1}{2}1}^A &= \sqrt{2K_+} \left(g_1 - \frac{M_{\mathbf{B}_i} - M_{\mathbf{B}_f}}{M_{\mathbf{B}_i}} g_2 \right), \\
 H_{\frac{1}{2}0}^A &= \frac{\sqrt{K_+}}{\sqrt{k^2}} \left(-(M_{\mathbf{B}_i} - M_{\mathbf{B}_f}) g_1 + \frac{k^2}{M_{\mathbf{B}_i}} g_2 \right), \\
 H_{\frac{1}{2}f}^A &= \frac{\sqrt{K_-}}{\sqrt{k^2}} \left(-(M_{\mathbf{B}_i} - M_{\mathbf{B}_f}) g_1 + \frac{k^2}{M_{\mathbf{B}_i}} g_3 \right), \quad (33)
 \end{aligned}$$

where $K_{\pm} = (M_{\mathbf{B}_i} - M_{\mathbf{B}_f})^2 - k^2$.

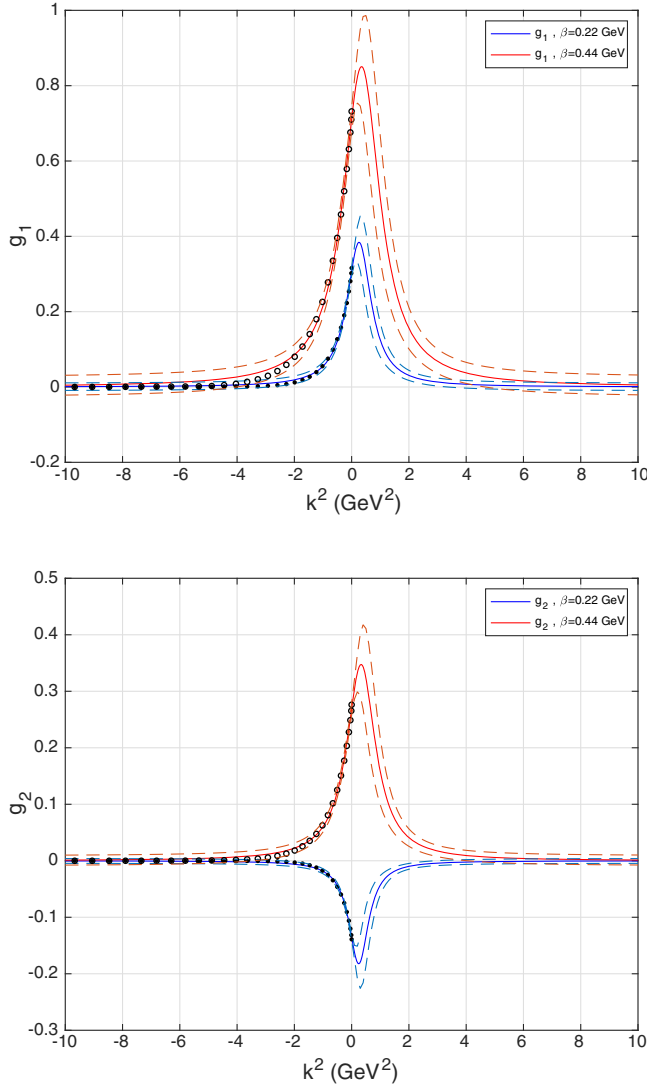

 FIG. 5. Legend is the same as Fig. 3 but for $\Lambda_c^+ \rightarrow n$.

 TABLE II. Fitting results of the form factors in LFCQM, where (I) and (II) represent the two scenarios of $\beta_{1I} = 0.22$ and $\beta_{1I} = 0.44$ for $\Lambda_c^+ \rightarrow n$, respectively.

$\Lambda_c^+ \rightarrow \Lambda$				
	f_1	f_2	g_1	g_2
$F(0)$	0.67 ± 0.01	0.76 ± 0.02	0.59 ± 0.01	$-(1.59 \pm 0.05) \times 10^{-3}$
q_1 (GeV $^{-2}$)	1.45 ± 0.29	1.42 ± 0.29	1.198 ± 0.26	0.53 ± 0.24
q_2 (GeV $^{-4}$)	2.39 ± 0.45	2.34 ± 0.44	1.904 ± 0.36	1.03 ± 0.23
$\Lambda_c^+ \rightarrow n$				
(I)	f_1	f_2	g_1	g_2
$F(0)$	0.34 ± 0.01	0.40 ± 0.01	0.30 ± 0.01	-0.14 ± 0.01
q_1 (GeV $^{-2}$)	1.79 ± 0.36	1.83 ± 0.37	1.56 ± 0.33	2.08 ± 0.41
q_2 (GeV $^{-4}$)	3.59 ± 0.68	3.65 ± 0.69	3.03 ± 0.56	4.24 ± 0.83
(II)	f_1	f_2	g_1	g_2
$F(0)$	0.83 ± 0.02	1.05 ± 0.02	0.71 ± 0.02	0.27 ± 0.01
q_1 (GeV $^{-2}$)	1.25 ± 0.26	1.20 ± 0.25	0.94 ± 0.22	1.37 ± 0.27
q_2 (GeV $^{-4}$)	1.85 ± 0.34	1.77 ± 0.33	1.36 ± 0.25	2.08 ± 0.28

The differential decay widths and asymmetries can be expressed in the analytic forms in terms of the helicity amplitudes, which can be found in Ref. [22]. In our numerical calculations, we use the center value of $\tau_{\Lambda_c^+} = 203.5 \times 10^{-15}$ s in Eq. (1) [1]. Our predictions of the decay branching ratios (\mathcal{B} s) and asymmetries (α s) are listed in Table IV. In Table V, we compare our results with the experimental data and various other calculations in the literature.

In LF [32] and the heavy effective theory (HQET) [26], the authors use a specific spin-flavor structure of $c(ud - du)\chi_{s_z}^{\rho_3}$ for the charmed baryon state, in which only the permutation relation is considered between light quarks. In addition, they assume that the diquarks from the light quark pairs are spectators and structureless. These simplifications make the results in Refs. [26,32] be not good compared with the experimental data as shown in Table V. Based on the Fermi statistics, the overall spin-flavor-momentum structures are determined, from which the parameters like quark masses, baryon masses, and shape parameters can recover the spin-flavor symmetry. It is interesting to see that when we consider scenario II in the neutron the same shape parameters of β_{QB} and β_{qB} in our study imply the totally symmetric momentum distribution of three constituent quarks in the baryon. In addition, the flavor symmetry breaking effect due to the quark masses seems to get canceled due to the clustering effect of the shape parameters in the momentum distribution functions. Our numerical results indicate that the form factors follow the Lorentzian functions of $F(k^2) = F(0)/(1 - q_1 k^2 + q_2 k^4)$ in both $\Lambda_c^+ \rightarrow \Lambda(n)$ processes. Our results of $f_i(k^2) \neq g_i(k^2)$ show that the heavy quark symmetry is broken because the constituent charm quark mass is not heavy enough.

TABLE III. Fitting results of the form factors in MBM.

	f_1	f_2	g_1	g_2
$\Lambda_c^+ \rightarrow \Lambda$	0.54	0.22	0.52	-0.06
$\Lambda_c^+ \rightarrow n$	0.40	0.22	0.43	-0.07

TABLE IV. Predictions of the decay branching ratios and asymmetry parameters in the LFCQM and MBM, where (I) and (II) represent the two scenarios of $\beta = 0.22$ and 0.44 for $\Lambda_c^+ \rightarrow n$, respectively.

	LFCQM		MBM	
	$\mathcal{B}(\%)$	α	$\mathcal{B}(\%)$	α
$\Lambda_c^+ \rightarrow \Lambda e^+ \nu_e$	3.36 ± 0.87	-0.97 ± 0.03	3.48	-0.83
$\Lambda_c^+ \rightarrow \Lambda \mu^+ \nu_\mu$	3.21 ± 0.85	-0.97 ± 0.03	3.38	-0.82
$\Lambda_c^+ \rightarrow n e^+ \nu_e$	0.057 ± 0.015 (I)	-0.98 ± 0.02 (I)	0.279	-0.87
	0.36 ± 0.15 (II)	-0.96 ± 0.04 (II)		
$\Lambda_c^+ \rightarrow n \mu^+ \nu_\mu$	0.054 ± 0.015 (I)	-0.98 ± 0.01 (I)	0.273	-0.87
	0.34 ± 0.14 (II)	-0.96 ± 0.04 (II)		

As shown in Table IV, we predict that $\mathcal{B}(\Lambda_c^+ \rightarrow \Lambda e^+ \nu_e) = (3.36 \pm 0.87) \times 10^{-2}$ and $\alpha(\Lambda_c^+ \rightarrow \Lambda e^+ \nu_e) = -0.96 \pm 0.03$, and $\mathcal{B}(\Lambda_c^+ \rightarrow n e^+ \nu_e) = (0.57 \pm 0.15, 3.6 \pm 1.5) \times 10^{-3}$, and $\alpha(\Lambda_c^+ \rightarrow n e^+ \nu_e) = (-0.98 \pm 0.02, -0.96 \pm 0.04)$ with the two scenarios of (I) and (II) in LFCQM, in which the value of $\mathcal{B}(\alpha)$ for the mode of $\Lambda_c^+ \rightarrow \Lambda e^+ \nu_e$ is lower (higher) than but acceptable by the experimental one $(3.6 \pm 0.4) \times 10^{-2} (-0.86 \pm 0.04)$ in PDG [2]. The errors in our results mainly come from the numerical fits of the MATLAB curve fitting toolbox given in Appendix, in which the 95% confidence bounds are broadened and tightened in the timelike and spacelike regions, respectively. Our

results are also consistent with those in LQCD [27,28], the relativistic quark model (RQM) [29], and the covariant confinement quark model (CCQM) [30,31]. For the MBM, although the semileptonic processes have been fully studied in Ref. [33], their results are mismatched with the current data. By using the same formalism with the same input parameters, we are able to get the same values of the form factors at the zero recoil point. By taking the Lorentzian k^2 dependences for the form factors, inspired from our LF calculations, we obtain much better results as shown in Table V. It is interesting to see that our results for $\Lambda_c^+ \rightarrow n e^+ \nu_e$ in LFCQM with scenario II is consistent with most of models. One the other hand, the prediction of scenario I is much smaller than those in the other calculations. This suppression comes from the wave function mismatching between the diquark in the charmed baryon and ordinary quark pairs in the neutron.

V. CONCLUSIONS

We have studied the semileptonic decays of $\Lambda_c^+ \rightarrow \Lambda(n) \ell^+ \nu_\ell$ in the two dynamical approaches of the LFCQM and MBM. We have used the Fermi statistics to determine the overall spin-flavor-momentum structures and recover the spin-flavor symmetry with the quark and baryon masses and shape parameters. We have found that $\mathcal{B}(\Lambda_c^+ \rightarrow \Lambda e^+ \nu_e) = (3.36 \pm 0.87)\%$ and 3.48% in the LFCQM and MBM, respectively, which are consistent with the experimental data of $(3.6 \pm 0.4) \times 10^{-2}$ [2] as well as the values predicted by $SU(3)_F$ [22], LQCD [27,28], RQM [29], and CCQM [30,31] but about a factor of 2 larger than those in HQET [26] and LF [32]. We have also obtained that $\alpha(\Lambda_c^+ \rightarrow \Lambda e^+ \nu_e) = (-0.97 \pm 0.03)$ and -0.83 in the LFCQM and MBM, which are lower and higher than the experimental data of -0.86 ± 0.04 [2],

TABLE V. Our results in comparisons with the experimental data and those in various calculations in the literature.

	$\Lambda_c^+ \rightarrow \Lambda e^+ \nu_e$		$\Lambda_c^+ \rightarrow n e^+ \nu_e$	
	$\mathcal{B}(\%)$	α	$\mathcal{B}(\%)$	α
LFCQM	3.36 ± 0.87	-0.97 ± 0.03	0.057 ± 0.015 (I) 0.36 ± 0.15 (II)	-0.98 ± 0.01 (I) -0.96 ± 0.04 (II)
MBM	3.48	-0.83	0.279	-0.87
Data [2]	3.6 ± 0.4	-0.86 ± 0.04
$SU(3)$ [22]	3.2 ± 0.3	-0.86 ± 0.04	0.51 ± 0.04	-0.89 ± 0.04
HQET [26]	1.42
LF [32]	1.63	...	0.201	...
MBM ^a [33]	2.6	...	0.20	...
NRQM [33]	3.2	...	0.30	...
LQCD [27,28]	3.80 ± 0.22	...	0.410 ± 0.029	...
RQM [29]	3.25	...	0.268	...
CCQM [30,31]	2.78	-0.87	0.202	...

^aAlthough the values of f_i and g_i are the same at the zero recoil point ($\vec{q} = 0$), we use the Lorentzian type of the k^2 dependences for the form factors instead of the dipole ones in this work.

respectively. We have predicted that $\mathcal{B}(\Lambda_c^+ \rightarrow ne^+\nu_e) = (0.57 \pm 0.15, 3.6 \pm 1.5) \times 10^{-3}$ and $\alpha(\Lambda_c^+ \rightarrow ne^+\nu_e) = (-0.98 \pm 0.02, -0.96 \pm 0.04)$ with the two different scenarios of (I, II) in the LFCQM and $\mathcal{B}(\Lambda_c^+ \rightarrow ne^+\nu_e) = 0.279 \times 10^{-2}$ and $\alpha(\Lambda_c^+ \rightarrow ne^+\nu_e) = -0.87$ in the MBM, in which our results of $\mathcal{B}(\Lambda_c^+ \rightarrow ne^+\nu_e)$ in the MBM and LFCQM (II) are consistent with those in the RQM [29] and CCQM [31] but about two times smaller than the values in $SU(3)_F$ [22] and LQCD [27,28]. On the other hand, our results of $\mathcal{B}(\Lambda_c^+ \rightarrow ne^+\nu_e)$ in the LFCQM (I) is much smaller than other calculations. This additional suppression could be understood by the wave function mismatching between the diquark and ordinary quark pairs. It is clear that our predicted values for the decay branching ratio and asymmetry in $\Lambda_c^+ \rightarrow ne^+\nu_e$ could be tested in the ongoing experiments at BESIII, LHCb, and BELLEII. Finally, we remark that our calculations in LFCQM and MBM can be also extended to the other charmed baryons, such as $\Xi_c^{+,0}$, and even b-baryons.

ACKNOWLEDGMENTS

This work was supported in part by National Center for Theoretical Sciences and MoST (Grant No. MoST-107-2119-M-007-013-MY3).

APPENDIX: FORM FACTORS IN THE LFCQM

We now show our numerical results for the form factors in Eqs. (21)–(24) in the LFCQM. In Fig. 2, we plot the vector form factors of $f_{1,2}$ with respect to the transfer momentum k^2 in the unit of GeV^2 for $\Lambda_c^+ \rightarrow \Lambda$, where the symbol of \bullet denotes the value calculated by Eqs. (21) and (23) from $k^2 = 0$ to -9.7 GeV^2 with *Mathematica*, while the blue line corresponds to the fitted function by the MATLAB curve fitting toolbox, and the dashed line represents the 95% confidence bounds (conf. bnds.) of the fit. Similarly, we depict the axial-vector form factors of $g_{1,2}$ in Fig. 3. The corresponding results for $\Lambda_c^+ \rightarrow n$ are given in Figs. 4 and 5.

-
- [1] R. Aaij *et al.* (LHCb Collaboration), *Phys. Rev. D* **100**, 032001 (2019).
 - [2] M. Tanabashi *et al.* (Particle Data Group), *Phys. Rev. D* **98**, 030001 (2018).
 - [3] Y. B. Li *et al.* (Belle Collaboration), *Phys. Rev. Lett.* **122**, 082001 (2019).
 - [4] Y. B. Li *et al.* (Belle Collaboration), *Phys. Rev. D* **100**, 031101 (2019).
 - [5] M. J. Savage and R. P. Springer, *Phys. Rev. D* **42**, 1527 (1990).
 - [6] M. J. Savage, *Phys. Lett. B* **257**, 414 (1991).
 - [7] C. D. Lu, W. Wang, and F. S. Yu, *Phys. Rev. D* **93**, 056008 (2016).
 - [8] C. Q. Geng, Y. K. Hsiao, C. W. Liu, and T. H. Tsai, *J. High Energy Phys.* **11** (2017) 147.
 - [9] W. Wang, Z. P. Xing, and J. Xu, *Eur. Phys. J. C* **77**, 800 (2017).
 - [10] C. Q. Geng, Y. K. Hsiao, Y. H. Lin, and L. L. Liu, *Phys. Lett. B* **776**, 265 (2018).
 - [11] C. Q. Geng, Y. K. Hsiao, C. W. Liu, and T. H. Tsai, *Phys. Rev. D* **97**, 073006 (2018).
 - [12] D. Wang, P. F. Guo, W. H. Long, and F. S. Yu, *J. High Energy Phys.* **03** (2018) 066.
 - [13] C. Q. Geng, Y. K. Hsiao, C. W. Liu, and T. H. Tsai, *Eur. Phys. J. C* **78**, 593 (2018).
 - [14] X. G. He and W. Wang, *Chin. Phys. C* **42**, 103108 (2018).
 - [15] X. G. He, Y. J. Shi, and W. Wang, *arXiv:1811.03480*.
 - [16] C. Q. Geng, Y. K. Hsiao, C. W. Liu, and T. H. Tsai, *Phys. Rev. D* **99**, 073003 (2019).
 - [17] C. Q. Geng, C. W. Liu, and T. H. Tsai, *Phys. Lett. B* **790**, 225 (2019).
 - [18] C. Q. Geng, C. W. Liu, and T. H. Tsai, *Phys. Lett. B* **794**, 19 (2019).
 - [19] C. Q. Geng, C. W. Liu, T. H. Tsai, and Y. Yu, *Phys. Rev. D* **99**, 114022 (2019).
 - [20] J. Y. Cen, C. Q. Geng, C. W. Liu, and T. H. Tsai, *Eur. Phys. J. C* **79**, 946 (2019).
 - [21] Y. K. Hsiao, Y. Yao, and H. J. Zhao, *Phys. Lett. B* **792**, 35 (2019).
 - [22] C. Q. Geng, C. W. Liu, T. H. Tsai, and S. W. Yeh, *Phys. Lett. B* **792**, 214 (2019).
 - [23] Y. Grossman and S. Schacht, *J. High Energy Phys.* **07** (2019) 020.
 - [24] S. Roy, R. Sinha, and N. G. Deshpande, *Phys. Rev. D* **101**, 036018 (2020).
 - [25] C. P. Jia, D. Wang, and F. S. Yu, *arXiv:1910.00876*.
 - [26] H. Y. Cheng and B. Tseng, *Phys. Rev. D* **53**, 1457 (1996).
 - [27] S. Meinel, *Phys. Rev. Lett.* **118**, 082001 (2017).
 - [28] S. Meinel, *Phys. Rev. D* **97**, 034511 (2018).
 - [29] R. N. Faustov and V. O. Galkin, *Eur. Phys. J. C* **76**, 628 (2016).
 - [30] T. Gutsche, M. A. Ivanov, J. G. Körner, V. E. Lyubovitskij, and P. Santorelli, *Phys. Rev. D* **93**, 034008 (2016).
 - [31] T. Gutsche, M. A. Ivanov, J. G. Körner, V. E. Lyubovitskij, and P. Santorelli, *Phys. Rev. D* **90**, 114033 (2014); **94**, 059902(E) (2016).
 - [32] Z. X. Zhao, *Chin. Phys. C* **42**, 093101 (2018).
 - [33] R. Perez-Marcial, R. Huerta, A. Garcia, and M. Avila-Aoki, *Phys. Rev. D* **40**, 2955 (1989); **44**, 2203(E) (1991).
 - [34] W. M. Zhang, *Chin. J. Phys.* **32**, 717 (1994).
 - [35] F. Schlumpf, *arXiv:hep-ph/9211255*.

- [36] C. Q. Geng, C. C. Lih, and W. M. Zhang, *Phys. Rev. D* **57**, 5697 (1998).
- [37] C. C. Lih, C. Q. Geng, and W. M. Zhang, *Phys. Rev. D* **59**, 114002 (1999).
- [38] C. Q. Geng, C. C. Lih, and W. M. Zhang, *Phys. Rev. D* **62**, 074017 (2000).
- [39] C. Q. Geng, C. W. Hwang, C. C. Lih, and W. M. Zhang, *Phys. Rev. D* **64**, 114024 (2001).
- [40] C. Q. Geng and C. C. Liu, *J. Phys. G* **29**, 1103 (2003).
- [41] H. Y. Cheng, C. K. Chua, and C. W. Hwang, *Phys. Rev. D* **69**, 074025 (2004).
- [42] H. Y. Cheng, C. K. Chua, and C. W. Hwang, *Phys. Rev. D* **70**, 034007 (2004).
- [43] C. Q. Geng, C. C. Lih, and C. Xia, *Eur. Phys. J. C* **76**, 313 (2016).
- [44] H. Y. Cheng and X. W. Kang, *Eur. Phys. J. C* **77**, 587 (2017); **77**, 863(E) (2017).
- [45] Z. X. Zhao, *Eur. Phys. J. C* **78**, 756 (2018).
- [46] Z. P. Xing and Z. X. Zhao, *Phys. Rev. D* **98**, 056002 (2018).
- [47] Q. Chang, L. T. Wang, and X. N. Li, *J. High Energy Phys.* **12** (2019) 102.
- [48] C. K. Chua, *Phys. Rev. D* **99**, 014023 (2019).
- [49] C. K. Chua, *Phys. Rev. D* **100**, 034025 (2019).
- [50] H. Y. Cheng and B. Tseng, *Phys. Rev. D* **46**, 1042 (1992); Erratum, *Phys. Rev. D* **55**, 1697 (1997).
- [51] H. Y. Cheng, X. W. Kang, and F. Xu, *Phys. Rev. D* **97**, 074028 (2018).
- [52] J. Zou, F. Xu, G. Meng, and H. Y. Cheng, *Phys. Rev. D* **101**, 014011 (2020).
- [53] H. W. Ke, N. Hao, and X. Q. Li, *Eur. Phys. J. C* **79**, 540 (2019).
- [54] H. W. Ke, X. Q. Li, and Z. T. Wei, *Phys. Rev. D* **77**, 014020 (2008).
- [55] H. W. Ke, X. H. Yuan, X. Q. Li, Z. T. Wei, and Y. X. Zhang, *Phys. Rev. D* **86**, 114005 (2012).
- [56] C. Lorce, B. Pasquini, and M. Vanderhaeghen, *J. High Energy Phys.* **05** (2011) 041.
- [57] W. N. Polyzou, W. Glockle, and H. Witala, *Few Body Syst.* **54**, 1667 (2013).
- [58] A. Bernotas and V. Simonis, *Nucl. Phys.* **A741**, 179 (2004).
- [59] A. Bernotas and V. Simonis, arXiv:1209.2900.
- [60] R. Jaffe and J. Kiskis, *Phys. Rev. D* **13**, 1355 (1976).
- [61] T. A. DeGrand, R. Jaffe, K. Johnson, and J. Kiskis, *Phys. Rev. D* **12**, 2060 (1975).
- [62] M. Betz and R. Goldflam, *Phys. Rev. D* **28**, 2848 (1983).
- [63] W. Jaus, *Phys. Rev. D* **44**, 2851 (1991).
- [64] W. Jaus, *Phys. Rev. D* **53**, 1349 (1996); **54**, 5904(E) (1996).
- [65] Q. Chang, X. N. Li, X. Q. Li, F. Su, and Y. D. Yang, *Phys. Rev. D* **98**, 114018 (2018).